https://doi.org/10.1016/j.apenergy.2018.04.024

Model Reduction Strategy of Doubly-fed Induction Generator-based Wind Farms for Power System Small-signal Rotor Angle Stability Analysis

S. W. Xia[a,b], S. Q. Bu[a*], X. Zhang[c], Y. Xu[d], B. Zhou[e] and J. B. Zhu[f]

[a] The Hong Kong Polytechnic University, Hung Hom, Kowloon, Hong Kong SAR

[b] North China Electric Power University, Changping District, Beijing 102206, China

[c] Electricity National Control Centre, National Grid, Wokingham RG41 5BN, UK

[d] Nanyang Technological University, 50 Nanyang Avenue, Singapore 639798

[e] Hunan University, Yuelushan, Changsha 410082, China

[f] Tianjin University, Nankai District, Tianjin 300072, China

***Abstract*—**Following the decarbonisation and decentralisation of energy industry, wind energy is becoming a promising generation source to reduce greenhouse emission, and meet future energy demand. Unlike traditional generation using synchronous generators, many wind turbines use induction generators, e.g., doubly-fed induction generators, due to the cost effective design of adjustable-speed operation and flexibility in reactive power control. However, a growing number of doubly-fed induction generator-based wind farms has significantly increased the complexity of system dynamic model, and hence increased the computational burden of power system dynamic study. This becomes a serious concern in the electricity system operation, where a fast power system stability assessment is required to assure the real-time system security during high levels of wind power penetration. In this paper, a novel model reduction strategy of doubly-fed induction generators is derived to improve the efficiency of power system dynamic study, while the study accuracy is still maintained to an acceptable level. To achieve this, a method to assess the modeling adequacy of doubly-fed induction generators for small-signal rotor angle stability analysis is firstly introduced. By evaluating the damping torque contribution to stability margin from different dynamic model components of doubly-fed induction generators, the proposed method provides a quantitative index (i.e., participation level) to show the involvement of each dynamic model component of doubly-fed induction generators in affecting power system damping, and thus can instruct how to reduce the model of doubly-fed induction generators in an efficient and accurate manner. On this basis, five model reduction plans and a model reduction strategy have been proposed according to the previously defined participation levels. The effectiveness of the proposed strategy is demonstrated in the New England test system and a real large power grid in Eastern China respectively. It has been proved that the proposed the model reduction strategy of doubly-fed induction generators for power system dynamic study is undoubtedly useful to the electricity system operator, with a key benefit in reducing model complexity and improving computational efficiency of a large-scale power system with an increasing number of wind power generation.

***Key Words*—**Computational efficiency; Damping torque contribution; Dynamic model component; Small-signal rotor angle stability; Reduced model; Wind energy.

NOMENCLATURE

DFIG doubly-fed induction generator

SG synchronous generator
RSC rotor-side converter
GSC grid-side converter
MRM model reduction margin
$\Delta \boldsymbol{X_w}$ vector of state variables of DFIGs
$\Delta \boldsymbol{X_g}$ vector of state variables associated with non-DFIG elements including SGs
$\Delta \boldsymbol{V_w}$ vector of terminal voltage associated with DFIG buses
$\Delta \boldsymbol{V_g}$ vector of terminal voltage associated with non-DFIG buses
$\boldsymbol{Y}$ admittance matrix of the system
$\Delta \boldsymbol{\delta}$ vector of variation of power angle of SGs
$\Delta \boldsymbol{\omega}$ vector of variation of angular speed of SGs
$\Delta \boldsymbol{z}$ vector of other state variables of SGs
$\Delta \boldsymbol{s}$ vector of variation of slip of DFIGs
$\Delta \boldsymbol{E_d}$ vector of variation of d-axis electromotive force of DFIGs
$\Delta \boldsymbol{E_q}$ vector of variation of q-axis electromotive force of DFIGs
$\Delta \boldsymbol{X_c}$ vector of state variables of converter integral controllers as well as the DC link of DFIGs

1. INTRODUCTION

Modern technologies, energy policies and business models are driving the transition of energy industry to a low-carbon [1,2] and decentralised future [3,4]. Wind energy plays a key role in facilitating such a transition by providing sustainable electricity to power grid with negligible carbon emission [5]. Following the decommissioning of fossil-fuel power generation, wind energy is also becoming a promising energy resource to meet future electricity demand [6,7]. As a result, most countries encourage the development of wind power generation capacity by significantly increasing the number and size of wind power generation connected to electricity grids [8,9].

The dominant type of wind power generation in the world market is doubly-fed induction generators (DFIGs), due to their cost effective design, the ability to operate at variable speed, and flexibility in reactive power dispatch [10]. Compared with conventional generation, DFIG-based wind power generation is equipped with power electronics converters, which enables its characteristic of a faster response and better control [11]. However, on the other hand, the converter controllers have also raised the modeling complexity and dimensionality of wind power generators [12]. As a result, the size of the dynamic model of a power system integrated with large numbers of DFIG-based wind farms could be considerably increased. Since the model size can significantly affect the efficiency of system dynamic study, especially for time-domain simulation, it is crucial to assess the modeling adequacy and reduce model complexity of DFIGs for power system small-signal rotor angle stability analysis.

The study of DFIG modeling for dynamic analysis could date back over ten years and quite a few efforts have been devoted to the work, which can be generally divided into two categories: the detailed dynamic modeling and model reduction for DFIGs. The detailed DFIG models [13,14] are widely used to study the dynamics of DFIG controllers and wind power generators' own stability issues [15,16]. In addition, the impact of DFIG integration on comparatively small-scale power system dynamics can be also analysed by the detailed DFIG models [17,18]. Different from the conventional vector control scheme, a phase angle controlled DFIG model is introduced in the study to support the stability of a 3-machine power system [17]. An enhanced DFIG dynamic model is proposed in [18] to investigate the impact of the ancillary service of a DFIG-based wind farm on the small-signal rotor angle stability of a 4-machine 2-area power system. On the other side, the reduced models retain certain aspects of DFIG

dynamic behaviors and are more suitable for the analysis of a large-scale power system with a high penetration level of wind power generation. Initially, most of reduced DFIG models are obtained by numerous trials of different models [19] and then validated by comparing the stability curves from time-consuming simulations [20,21]. Later some theoretical model order reduction techniques are developed to derive the reduced DFIG models, e.g., selective modal analysis in [22] and balanced truncation in [23]. Then these techniques are further used to establish the aggregate model for DFIG-based wind farms, such as selective modal analysis in [24] and singular perturbation analysis in [25]. However, most of model reductions mentioned above only focus on reduction impact on the dynamics of DFIG itself (e.g., wind power output), which might not meet the requirement of the electricity system operator, whose responsibility is to analyse the dynamic performance of the overall system. Hence, besides time-consuming trials by the modal analysis and time domain simulation, there is no study seen to deal with the DFIG model reduction from the perspective of the whole system impact (e.g., the impact on the system small-signal rotor angle stability and inter-area electromechanical oscillation modes). Moreover, the existing publications have not yet addressed all the reduction possibilities according to different system operational conditions.

In this paper, a novel model reduction strategy for DFIGs based on the proposed modeling adequacy assessment is presented, which is applicable to both the individual DFIG model and wind farm aggregate model. The main contributions of this paper are clarified as follows: 1. Compared with the existing participation factor from the modal analysis [26], the proposed eigenvalue-oriented quantitative index (i.e., participation level) from damping torque analysis is more accurate in assessing the damping performance of each DFIG dynamic model component as the damping is essentially the decaying rate of the oscillation, which is related to the real part of the eigenvalue. If the participation factor can assess the damping in a qualitative manner, the proposed participation level can assess the damping in a quantitative manner; 2. Compared with the existing damping torque calculation method proposed in [27], the proposed modeling adequacy assessment can facilitate the understanding of each internal component of DFIG dynamic model and their damping contribution mechanism to small-signal rotor angle stability analysis; 3. The model reduction strategy can indicate how to efficiently reduce the DFIG model complexity by recommending which model component(s) of DFIG can be certainly ignored, while still maintain the modeling accuracy and adequacy to an acceptable level; 4. The model reduction strategy not only aims to simplify each individual DFIG model, but most importantly also aims to further reduce the aggregate models of wind farms on top of the equivalent aggregate model strategy (e.g., [24][25]) as a second-stage reduction strategy; 5. The work provides electricity system operator with a practical tool that could significantly reduce the study time and calculation burden for power system dynamic study, which is particularly useful when dealing with fast on-line stability calculation with high penetration levels of wind energy.

The paper is organized as follows. In Section 2, a method to assess the modeling adequacy of DFIGs for the study of system critical oscillation mode is firstly introduced. The participation level of each order of DFIG dynamic model in damping contributions to the electromechanical loop of synchronous generators (SGs) is assessed respectively. In Section 3, a model reduction strategy of DFIGs for small-signal rotor angle stability analysis is proposed, and five reduced dynamic models with their linearised forms are derived according to five participation level conditions from the previous modeling adequacy assessment. Two case studies are presented in Section 4, where the proposed model reduction strategy and modeling adequacy assessment of DFIGs are validated by modal analysis and time-domain simulation. Finally, two typical applications of the presented work are discussed in Section 5.

2. MODELING ADEQUACY ASSESSMENT OF DOUBLY-FED INDUCTION GENERATORS

2.1 Internal Dynamic Model of Doubly-fed Induction Generators

Fig. 1 shows the structure of a DFIG-based wind power generation. The major components include an induction generator, the stator of which is directly connected to power grid, and the rotor of which is connected to power grid via a back-to-back converter. The back-to-back convertor consists of two independent convertors, namely rotor-side converter (RSC) and grid-side converter (GSC) controller, which are equipped with a DC link to bridge them. The convertors and their associated controllers govern the performance of the DFIG, and provide variable speed operation and dynamic response subjected to power grid disturbance.

The complete dynamic model of DFIGs consists of the internal dynamic model and algebraic interface equations of DFIGs, the latter part of which indicates how DFIGs are interfaced with the grid and will be introduced in the next subsection. The internal dynamic model includes dynamics of the induction generator, RSC controller, GSC controller and DC link, which can be represented by a set of first-order differential equations [13-18]. The stator transient of DFIGs as well as the wind turbine shaft dynamics can be ignored when the study focus is on the system electromechanical oscillation mode [28,29]. The generic format of the internal dynamic model of DFIGs by using linearised differential equations can be written as [26]

$$\Delta\dot{\boldsymbol{X}}_{\boldsymbol{w}} = \boldsymbol{A}_{\boldsymbol{w}}\Delta\boldsymbol{X}_{\boldsymbol{w}} + \boldsymbol{B}_{\boldsymbol{w}}\Delta\boldsymbol{V}_{\boldsymbol{w}} \tag{1}$$

where $\Delta\boldsymbol{X}_{\boldsymbol{w}}$ is the vector of state variables of DFIGs, $\Delta\boldsymbol{V}_{\boldsymbol{w}}$ is the vector of terminal voltage associated with DFIG buses, and $\boldsymbol{A}_{\boldsymbol{w}}$ and $\boldsymbol{B}_{\boldsymbol{w}}$ are the matrices in the internal dynamic model of DFIGs associated with $\Delta\boldsymbol{X}_{\boldsymbol{w}}$ and $\Delta\boldsymbol{V}_{\boldsymbol{w}}$ respectively. The detailed format of (1) can be expressed as

$$\begin{bmatrix} \Delta\dot{\boldsymbol{s}} \\ \Delta\dot{\boldsymbol{E}}_{\boldsymbol{d}} \\ \Delta\dot{\boldsymbol{E}}_{\boldsymbol{q}} \\ \Delta\dot{\boldsymbol{X}}_{\boldsymbol{c}} \end{bmatrix} = \begin{bmatrix} \boldsymbol{A}_{\boldsymbol{11w}} & \boldsymbol{A}_{\boldsymbol{12w}} & \boldsymbol{0} & \boldsymbol{0} \\ \boldsymbol{0} & \boldsymbol{A}_{\boldsymbol{22w}} & \boldsymbol{0} & \boldsymbol{A}_{\boldsymbol{24w}} \\ \boldsymbol{0} & \boldsymbol{0} & \boldsymbol{A}_{\boldsymbol{33w}} & \boldsymbol{A}_{\boldsymbol{34w}} \\ \boldsymbol{A}_{\boldsymbol{41w}} & \boldsymbol{A}_{\boldsymbol{42w}} & \boldsymbol{A}_{\boldsymbol{43w}} & \boldsymbol{A}_{\boldsymbol{44w}} \end{bmatrix} \begin{bmatrix} \Delta\boldsymbol{s} \\ \Delta\boldsymbol{E}_{\boldsymbol{d}} \\ \Delta\boldsymbol{E}_{\boldsymbol{q}} \\ \Delta\boldsymbol{X}_{\boldsymbol{c}} \end{bmatrix} + \begin{bmatrix} \boldsymbol{B}_{\boldsymbol{1w}} \\ \boldsymbol{B}_{\boldsymbol{2w}} \\ \boldsymbol{B}_{\boldsymbol{3w}} \\ \boldsymbol{B}_{\boldsymbol{4w}} \end{bmatrix} \Delta\boldsymbol{V}_{\boldsymbol{w}} \tag{2}$$

where $\Delta\boldsymbol{s}$, $\Delta\boldsymbol{E}_{\boldsymbol{d}}$ and $\Delta\boldsymbol{E}_{\boldsymbol{q}}$ are the vectors of the slip and electromotive force of DFIGs, and $\Delta\boldsymbol{X}_{\boldsymbol{c}}$ is the vector of the state variables of converter integral controllers as well as the DC link of DFIGs. $\boldsymbol{A}_{\boldsymbol{11w}}$, $\boldsymbol{A}_{\boldsymbol{12w}}$, $\boldsymbol{A}_{\boldsymbol{22w}}$, $\boldsymbol{A}_{\boldsymbol{24w}}$, $\boldsymbol{A}_{\boldsymbol{33w}}$, $\boldsymbol{A}_{\boldsymbol{34w}}$, $\boldsymbol{A}_{\boldsymbol{41w}}$, $\boldsymbol{A}_{\boldsymbol{42w}}$, $\boldsymbol{A}_{\boldsymbol{43w}}$ and $\boldsymbol{A}_{\boldsymbol{44w}}$ are the sub-matrices of $\boldsymbol{A}_{\boldsymbol{w}}$ corresponding to different state variables of DFIGs.

2.2 Dynamic Model of a Multi-machine Power System with Algebraic Interface Equations of Doubly-fed Induction Generators

A standard procedure to establish the linearised dynamic model of a multi-machine power system with algebraic interface equations of DFIGs is applied [26].

$$\Delta\dot{\boldsymbol{X}}_{\boldsymbol{g}} = \boldsymbol{A}_{\boldsymbol{g}}\Delta\boldsymbol{X}_{\boldsymbol{g}} + [\boldsymbol{B}_{\boldsymbol{g}} \quad \boldsymbol{0}] \begin{bmatrix} \Delta\boldsymbol{V}_{\boldsymbol{g}} \\ \Delta\boldsymbol{V}_{\boldsymbol{w}} \end{bmatrix}$$

$$\boldsymbol{0} = \begin{bmatrix} -\boldsymbol{C}_{\boldsymbol{g}} & \boldsymbol{0} \\ \boldsymbol{0} & -\boldsymbol{C}_{\boldsymbol{w}} \end{bmatrix} \begin{bmatrix} \Delta\boldsymbol{X}_{\boldsymbol{g}} \\ \Delta\boldsymbol{X}_{\boldsymbol{w}} \end{bmatrix} + \begin{bmatrix} \boldsymbol{Y}_{\boldsymbol{g}} - \boldsymbol{D}_{\boldsymbol{g}} & \boldsymbol{Y}_{\boldsymbol{gw}} \\ \boldsymbol{Y}_{\boldsymbol{wg}} & \boldsymbol{Y}_{\boldsymbol{w}} - \boldsymbol{D}_{\boldsymbol{w}} \end{bmatrix} \begin{bmatrix} \Delta\boldsymbol{V}_{\boldsymbol{g}} \\ \Delta\boldsymbol{V}_{\boldsymbol{w}} \end{bmatrix}$$

(3)

where $\Delta \boldsymbol{X_g}$ is the vector of state variables associated with non-DFIG elements including SGs. DFIGs are connected to the buses ranking last in the system. $\Delta \boldsymbol{V_g}$ is the vector of terminal voltage associated with non-DFIG buses. $\boldsymbol{Y}$ is the admittance matrix of the system and the self-explanatory subscripts of $\boldsymbol{Y}$ define the sub-matrices corresponding to non-DFIG and DFIG elements respectively. $\boldsymbol{A_g}$ and $\boldsymbol{C_g}$ are the matrices associated with $\Delta \boldsymbol{X_g}$, and $\boldsymbol{B_g}$ and $\boldsymbol{D_g}$ are the matrices associated with $\Delta \boldsymbol{V_g}$ respectively in the dynamic model of a multi-machine power system. $\boldsymbol{D_w}$ is the matrix associated with $\Delta \boldsymbol{V_w}$ in the algebraic interface equations of DFIGs.

By eliminating the terminal voltage $\Delta \boldsymbol{V_w}$ in (3), it can have

$$\Delta \dot{\boldsymbol{X}}_{\boldsymbol{g}} = \boldsymbol{A_g}\Delta \boldsymbol{X_g} - \boldsymbol{B}\boldsymbol{D^{-1}}\boldsymbol{C}\begin{bmatrix}\Delta \boldsymbol{X_g} \\ \Delta \boldsymbol{X_w}\end{bmatrix} = \left(\boldsymbol{A_g} - [\boldsymbol{B}\boldsymbol{D^{-1}}\boldsymbol{C}]_{\boldsymbol{g}}\right)\Delta \boldsymbol{X_g} - [\boldsymbol{B}\boldsymbol{D^{-1}}\boldsymbol{C}]_{\boldsymbol{w}}\Delta \boldsymbol{X_w} \tag{4}$$

where $\boldsymbol{B} = [\boldsymbol{B_g} \quad \boldsymbol{0}]$, $\boldsymbol{C} = \begin{bmatrix}-\boldsymbol{C_g} & \boldsymbol{0} \\ \boldsymbol{0} & -\boldsymbol{C_w}\end{bmatrix}$, and $\boldsymbol{D} = \begin{bmatrix}\boldsymbol{Y_g} - \boldsymbol{D_g} & \boldsymbol{Y_{gw}} \\ \boldsymbol{Y_{wg}} & \boldsymbol{Y_w} - \boldsymbol{D_w}\end{bmatrix}$. $[\boldsymbol{B}\boldsymbol{D^{-1}}\boldsymbol{C}]_{\boldsymbol{g}}$ denotes the columns associated with $\Delta \boldsymbol{X_g}$ and $[\boldsymbol{B}\boldsymbol{D^{-1}}\boldsymbol{C}]_{\boldsymbol{w}}$ is associated with $\Delta \boldsymbol{X_w}$.

Equation (4) treats the state variables $\Delta \boldsymbol{X_w}$ of DFIGs as controllable variables. It can be seen from (4) that the impact of grid connection of DFIGs on the system dynamics mainly consists of two aspects, i.e., the superimposing of the admittance matrix $\boldsymbol{D_w}$ of DFIGs to the original non-DFIG matrix $\left(\boldsymbol{A_g} - [\boldsymbol{B}\boldsymbol{D^{-1}}\boldsymbol{C}]_{\boldsymbol{g}}\right)$ (which is related to the algebraic interface equations of DFIGs) and the contribution of state variable $\Delta \boldsymbol{X_w}$ of DFIG dynamics (which is related to the internal dynamic model of DFIGs). The two types of impact can be investigated separately in the small-signal rotor angle stability analysis. However, the latter impact might raise the computational cost in the real-time operation due to the increasing numbers of DFIGs which enlarge the dimension of system dynamic model. Equation (4) can be extended to its full representation as

$$\begin{bmatrix}\Delta \dot{\boldsymbol{\delta}} \\ \Delta \dot{\boldsymbol{\omega}} \\ \Delta \dot{\boldsymbol{z}}\end{bmatrix} = \begin{bmatrix}\boldsymbol{0} & \boldsymbol{\omega_0 I} & \boldsymbol{0} \\ \boldsymbol{A_{21}} & \boldsymbol{A_{22}} & \boldsymbol{A_{23}} \\ \boldsymbol{A_{31}} & \boldsymbol{A_{32}} & \boldsymbol{A_{33}}\end{bmatrix}\begin{bmatrix}\Delta \boldsymbol{\delta} \\ \Delta \boldsymbol{\omega} \\ \Delta \boldsymbol{z}\end{bmatrix} + \left[\begin{array}{c|c}\boldsymbol{0} & \\ \boldsymbol{B_2} & \boldsymbol{0} \\ \boldsymbol{B_3} & \end{array}\right]\left[\begin{array}{c}\Delta \boldsymbol{s} \\ \Delta \boldsymbol{E_d} \\ \Delta \boldsymbol{E_q} \\ \hline \Delta \boldsymbol{X_c}\end{array}\right] \tag{5}$$

where $\Delta \boldsymbol{\delta}$ and $\Delta \boldsymbol{\omega}$ are the vectors of the power angle and angular speed of SGs respectively, and $\Delta \boldsymbol{z}$ is the vector of other state variables of SGs. $\Delta \boldsymbol{s}$, $\Delta \boldsymbol{E_d}$ and $\Delta \boldsymbol{E_q}$ are the vectors of the slip and electromotive force of DFIGs. $\Delta \boldsymbol{X_c}$ is the vector of state variables of converter integral controllers as well as the DC link of DFIGs, the dimension of which could vary with the number of integral controller adopted as the proportional controller of the DFIG converter does not have its own state variable and is not described by the dynamic model of DFIG converter controller. It can be noted from the matrix expansion that $\Delta \boldsymbol{X_c}$ (refers to the dynamics of integral controller and DC link) does not have a direct contribution to the system damping unlike the other three state variables associated with the induction generator. $\boldsymbol{A_{21}}$, $\boldsymbol{A_{22}}$, $\boldsymbol{A_{23}}$, $\boldsymbol{A_{31}}$, $\boldsymbol{A_{32}}$ and $\boldsymbol{A_{33}}$ are sub-matrices of $\boldsymbol{A_g} - [\boldsymbol{B}\boldsymbol{D^{-1}}\boldsymbol{C}]_{\boldsymbol{g}}$ in (4) corresponding to different state variables of non-DFIG elements. $\boldsymbol{B_2}$ and $\boldsymbol{B_3}$ are sub-matrices of $\boldsymbol{B}\boldsymbol{D^{-1}}\boldsymbol{C}$ in (4) corresponding to different state variables of non-DFIG elements in row and $\Delta \boldsymbol{s}$, $\Delta \boldsymbol{E_d}$ and $\Delta \boldsymbol{E_q}$ in column.

2.3 Dynamic Interactions between Synchronous Generators and Doubly-fed Induction Generators in a Multi-machine Power System

Converting (1) to frequency domain, it can obtain

$$\Delta \boldsymbol{X_w} = (p\boldsymbol{I} - \boldsymbol{A_w})^{-1}\boldsymbol{B_w}\Delta \boldsymbol{V_w} \tag{6}$$

Equation (6) reveals that the internal dynamics of DFIGs can be regarded as a multi-input multi-output (MIMO) controller with transfer function $(p\boldsymbol{I} - \boldsymbol{A_w})^{-1}\boldsymbol{B_w}$. The physical insight is that if there is any system disturbance causing the terminal voltage variation $\Delta \boldsymbol{V_w}$ (input signal), DFIGs should have a dynamic response reflected by the state variable variation $\Delta \boldsymbol{X_w}$ (output signal), which is determined by the internal dynamic model of DFIGs. Then $\Delta \boldsymbol{X_w}$ will in turn affect the SGs and system according to (4) or (5), which generally demonstrates a dynamic interaction mechanism between DFIGs and SGs. Combining (4) and (6) together, the complete linearised model of a multi-machine power system with DFIGs is established.

2.4 Modeling Adequacy Assessment of Doubly-fed Induction Generators

Based on the established linearised model, a method to assess the modeling adequacy of DFIGs for the analysis of system critical oscillation mode is proposed below. The proposed assessment is carried out in the frequency domain, which can facilitate the derivation of damping contributions from the dynamic model components of DFIGs.

The multi-machine power system dynamic model presented in (5) can be also illustrated by Fig. 2 in frequency domain.

According to Fig. 2, the forward path function from $\left[\Delta \boldsymbol{s}, \Delta \boldsymbol{E_d}, \Delta \boldsymbol{E_q}\right]^{\boldsymbol{T}}$ to electric torque of SGs is

$$\boldsymbol{F_w}(p) = \boldsymbol{A_{23}}(p\boldsymbol{I} - \boldsymbol{A_{33}})^{-1}\boldsymbol{B_3} + \boldsymbol{B_2} \tag{7}$$

where $\boldsymbol{F_w}(p)$ is a $m \times 3l$ matrix, assuming there are totally m SGs and l DFIGs in the system.

From internal dynamic model of DFIG, (2) can be also illustrated by Fig. 3 in frequency domain. Hence, the contributions from $\Delta \boldsymbol{V_w}$ (input of DFIGs) to $\left[\Delta \boldsymbol{s}, \Delta \boldsymbol{E_d}, \Delta \boldsymbol{E_q}\right]^{\boldsymbol{T}}$ (output of DFIGs) can be computed and the dynamics of DFIGs can be split and described by three separate transfer functions

$$\begin{cases} \boldsymbol{G_{E_d}}(p) = [\boldsymbol{I} - (p\boldsymbol{I} - \boldsymbol{A_{22w}})^{-1}\boldsymbol{A_{24w}}(p\boldsymbol{I} - \boldsymbol{A_{44w}})^{-1}\boldsymbol{A_{42w}}]^{-1} \\ \qquad\qquad \times (p\boldsymbol{I} - \boldsymbol{A_{22w}})^{-1}[\boldsymbol{A_{24w}}(p\boldsymbol{I} - \boldsymbol{A_{44w}})^{-1}\boldsymbol{B_{4w}} + \boldsymbol{B_{2w}}] \\ \boldsymbol{G_{E_q}}(p) = [\boldsymbol{I} - (p\boldsymbol{I} - \boldsymbol{A_{33w}})^{-1}\boldsymbol{A_{34w}}(p\boldsymbol{I} - \boldsymbol{A_{44w}})^{-1}\boldsymbol{A_{43w}}]^{-1} \\ \qquad\qquad \times (p\boldsymbol{I} - \boldsymbol{A_{33w}})^{-1}[\boldsymbol{A_{34w}}(p\boldsymbol{I} - \boldsymbol{A_{44w}})^{-1}\boldsymbol{B_{4w}} + \boldsymbol{B_{3w}}] \\ \boldsymbol{G_s}(p) = (p\boldsymbol{I} - \boldsymbol{A_{11w}})^{-1}\left[\boldsymbol{B_{1w}} + \boldsymbol{A_{12w}}\boldsymbol{G_{E_d}}(p)\right] \end{cases} \tag{8}$$

where $\boldsymbol{G_{E_d}}(p)_{l\times 2l} = \Delta \boldsymbol{E_d}/\Delta \boldsymbol{V_w}$, $\boldsymbol{G_{E_q}}(p)_{l\times 2l} = \Delta \boldsymbol{E_q}/\Delta \boldsymbol{V_w}$, and $\boldsymbol{G_s}(p)_{l\times 2l} = \Delta \boldsymbol{s}/\Delta \boldsymbol{V_w}$. As proved by (5) previously that the dynamics of integral controllers and DC link of DFIG converter does not have a direct impact on the system damping, it actually contributes the system damping via the channel of $\left[\Delta \boldsymbol{s}, \Delta \boldsymbol{E_d}, \Delta \boldsymbol{E_q}\right]^{\boldsymbol{T}}$ as shown in Fig. 3. Therefore, both damping contributions of $\Delta \boldsymbol{E_d}$ and $\Delta \boldsymbol{E_q}$ consist of two parts, i.e., the contributions from their

own dynamics ($\Delta \boldsymbol{E_d}$ or $\Delta \boldsymbol{E_q}$) and dynamics of $\Delta \boldsymbol{X_c}$. It is easy to differentiate these two parts in $\boldsymbol{G_{E_d}}(p)$ and $\boldsymbol{G_{E_q}}(p)$ as well as $\boldsymbol{G_s}(p)$

$$\begin{cases} \boldsymbol{G_{E_d\_E_d}}(p) = (p\boldsymbol{I} - \boldsymbol{A_{22w}})^{-1}\boldsymbol{B_{2w}} \\ \boldsymbol{G_{E_d\_X_c}}(p) = \boldsymbol{G_{E_d}}(p) - \boldsymbol{G_{E_d\_E_d}}(p) \\ \boldsymbol{G_{E_q\_E_q}}(p) = (p\boldsymbol{I} - \boldsymbol{A_{33w}})^{-1}\boldsymbol{B_{3w}} \\ \boldsymbol{G_{E_q\_X_c}}(p) = \boldsymbol{G_{E_q}}(p) - \boldsymbol{G_{E_q\_E_q}}(p) \\ \boldsymbol{G_{s\_sE_d}}(p) = (p\boldsymbol{I} - \boldsymbol{A_{11w}})^{-1}\left[\boldsymbol{B_{1w}} + \boldsymbol{A_{12w}}\boldsymbol{G_{E_d\_E_d}}(p)\right] \\ \boldsymbol{G_{s\_X_c}}(p) = (p\boldsymbol{I} - \boldsymbol{A_{11w}})^{-1}\,\boldsymbol{A_{12w}}\boldsymbol{G_{E_d\_X_c}}(p) \end{cases} \tag{9}$$

Combining (7) and (8), the total electric torque provided by DFIGs to electromechanical oscillation loop of SGs in the system can be obtained

$$\Delta \boldsymbol{T_w} = \boldsymbol{F_w}(p)\begin{bmatrix} \boldsymbol{G_s}(p) \\ \boldsymbol{G_{E_d}}(p) \\ \boldsymbol{G_{E_q}}(p) \end{bmatrix}\Delta \boldsymbol{V_w} \tag{10}$$

where $\Delta \boldsymbol{T_w}$ denotes the electric torque contribution of DFIGs to all SGs and thus is a m-dimention vector. Assuming the i^{th} eigenvalue λ_i is the critical oscillation mode in the system, $\Delta \boldsymbol{V_w}$ should be equal to $\boldsymbol{\gamma_{ik}}\Delta\omega_k$ (see Appendix A.1), and thus the electric torque provided by DFIGs to the k^{th} SG (the k^{th} element of $\Delta \boldsymbol{T_w}$) can be rewritten as

$$\Delta T_{wk} = \boldsymbol{F_{wk}}(\lambda_i)\begin{bmatrix} \boldsymbol{G_s}(\lambda_i) \\ \boldsymbol{G_{E_d}}(\lambda_i) \\ \boldsymbol{G_{E_q}}(\lambda_i) \end{bmatrix}\boldsymbol{\gamma_{ik}}\Delta\omega_k \tag{11}$$

where $\boldsymbol{F_{wk}}(\lambda_i)$ is the k^{th} row of $\boldsymbol{F_w}(\lambda_i)$. Equation (11) can be further factorized to the torque contribution of the dynamic model components of each DFIG. The electric torque from different dynamics of the j^{th} DFIG to the k^{th} SG is

$$\begin{cases} \Delta T_{wkj\_s} = F_{wkj\_s}(\lambda_i)\boldsymbol{G_{s\_sE_dj}}(\lambda_i)\boldsymbol{\gamma_{ijk}}\Delta\omega_k \\ \Delta T_{wkj\_E_d} = F_{wkj\_E_d}(\lambda_i)\boldsymbol{G_{E_d\_E_dj}}(\lambda_i)\boldsymbol{\gamma_{ijk}}\Delta\omega_k \\ \Delta T_{wkj\_E_q} = F_{wkj\_E_q}(\lambda_i)\boldsymbol{G_{E_q\_E_qj}}(\lambda_i)\boldsymbol{\gamma_{ijk}}\Delta\omega_k \\ \Delta T_{wkj\_X_c} = \begin{bmatrix} F_{wkj\_E_d}(\lambda_i)\boldsymbol{G_{E_d\_X_cj}}(\lambda_i) \\ +F_{wkj\_E_q}(\lambda_i)\boldsymbol{G_{E_q\_X_cj}}(\lambda_i) \\ +F_{wkj\_s}(\lambda_i)\boldsymbol{G_{s\_X_cj}}(\lambda_i) \end{bmatrix}\boldsymbol{\gamma_{ijk}}\Delta\omega_k \end{cases} \tag{12}$$

where the subscript j, s, E_d, E_q and X_c denote the relevant part of matrices associated with different dynamics of the j^{th} DFIG.

As the electric torque contribution from the j^{th} DFIG to the k^{th} SG is the linear superposition of each component, $\Delta T_{wkj} = \Delta T_{wkj\_s} + \Delta T_{wkj\_E_d} + \Delta T_{wkj\_E_q} + \Delta T_{wkj\_X_c}$. Similarly, considering the contributions from all the DFIGs, the electric torque of the k^{th} SG $\Delta T_{wk} = \sum_{j=1}^{l} \Delta T_{wkj}$. Hence, the impact of DFIG dynamics on the i^{th} eigenvalue λ_i can be assessed in (13) by introducing S_{ik} (the sensitivity of λ_i with respect to the electric torque coefficient of the k^{th} SG, see Appendix A.2), so that the modeling adequacy assessment associated with the eigenvalue variation becomes a closed-loop design including the forward path function in (7), transfer function of DFIGs in (9) and eigenvalue sensitivity S_{ik}.

$$\Delta\lambda_i = \sum_{k=1}^{m} S_{ik} TC_{wk} = \sum_{k=1}^{m} S_{ik} \sum_{j=1}^{l} TC_{wkj}$$

$$= \sum_{k=1}^{m} S_{ik} \sum_{j=1}^{l} \left(TC_{wkj_s} + TC_{wkj_{E_d}} + TC_{wkj_{E_q}} + TC_{wkj_{X_c}} \right)$$

$$= \sum_{j=1}^{l} \left(\sum_{k=1}^{m} S_{ik} TC_{wkj_s} + \sum_{k=1}^{m} S_{ik} TC_{wkj_{E_d}} + \sum_{k=1}^{m} S_{ik} TC_{wkj_{E_q}} + \sum_{k=1}^{m} S_{ik} TC_{wkj_{X_c}} \right)$$

$$= \sum_{j=1}^{l} \left(PL_{j_s} + PL_{j_{E_d}} + PL_{j_{E_q}} + PL_{j_{X_c}} \right) \tag{13}$$

where TC_{wk} and TC_{wkj} are the electric torque coefficients of ΔT_{wk} and ΔT_{wkj}, and $TC_{wkj\_s}, TC_{wkj\_E_d}, TC_{wkj\_E_q}$ and $TC_{wkj\_X_c}$ are the electric torque coefficients of each dynamic model component before $\Delta\omega_k$ in (12). $PL_{j_s}, PL_{j_{E_d}}, PL_{j_{E_q}}$ and $PL_{j_{X_c}}$ represent the participation level of each dynamic model component of the j^{th} DFIG in affecting system critical eigenvalue and hence damping performance (which is called 'participation level' for short in the rest of the paper).

Based on the derivation above, the participation level defined by the contribution of each dynamic model component to the critical eigenvalue can be quantified by using (13). The participation level is able to indicate which part of DFIG dynamics can be ignored in the small-signal rotor angle stability analysis due to less involvement in dynamic interactions, and thus a method to determine the adequate model of DFIGs is established. The proposed method of modeling adequacy assessment only needs to implement the computation program once, in contrast to the existing methods that use arbitrary trials of comparing different DFIG models in model analysis or time-domain simulation. According to the assessment results, suitable model reduction plans can be made. Therefore, on the basis of the assessment method presented in this section, a model reduction strategy of DFIGs for small-signal rotor angle stability analysis is proposed in Section 3.

3. MODEL REDUCTION STRATEGY OF DOUBLY-FED INDUCTION GENERATORS

3.1 Participation Level Based Model Reduction Plans (Generator Level)

Based on different participation levels of the dynamic model components of DFIGs from the proposed modeling adequacy assessment, five model reduction plans of DFIG internal dynamic model for small-signal rotor angle stability analysis are established step by step in the following. Analogue to the simplification of SG model, the reduction of DFIG model starts from the detailed model and then all the reduction possibilities that have a clear physical insight are exhausted and considered.

1) Reduction of dynamics of $\Delta \boldsymbol{X_c}$ (constant $\boldsymbol{X_c}$ model)

$\Delta \boldsymbol{X_c}$ (the dynamics of integral controller and DC link only) impacts the system indirectly by contributing damping to $\Delta \boldsymbol{s}, \Delta \boldsymbol{E_d}$ and $\Delta \boldsymbol{E_q}$ (Fig. 3). If $\Delta \boldsymbol{X_c}$ has a high participation in affecting small-signal rotor angle stability margin which cannot be ignored, the dynamic model of $\left[\Delta \boldsymbol{s}, \Delta \boldsymbol{E_d}, \Delta \boldsymbol{E_q}\right]^{\boldsymbol{T}}$ cannot be reduced. In other words, only when the participation level of $\Delta \boldsymbol{X_c}$ is low, the multiple generator-level model reduction plans of DFIGs can be implemented. Therefore, the reduction of dynamics of $\Delta \boldsymbol{X_c}$ is considered as the first step of the DFIG model reduction on the generator level.

For demonstration purposes, in the rest of this subsection assume there is only one DFIG in the system. When the participation level of $\Delta \boldsymbol{X_c}$ is below certain threshold, the dynamics of $\Delta \boldsymbol{X_c}$ can be neglected and the linearised dynamic model in (2) is reduced to

$$\begin{bmatrix} \Delta \dot{s} \\ \Delta \dot{E}_d \\ \Delta \dot{E}_q \end{bmatrix} = \begin{bmatrix} A_{11w} & A_{12w} & 0 \\ 0 & A_{22w} & 0 \\ 0 & 0 & A_{33w} \end{bmatrix} \begin{bmatrix} \Delta s \\ \Delta E_d \\ \Delta E_q \end{bmatrix} + \begin{bmatrix} \boldsymbol{B_{1w}} \\ \boldsymbol{B_{2w}} \\ \boldsymbol{B_{3w}} \end{bmatrix} \Delta \boldsymbol{V_w} \tag{14}$$

Hence, the transfer function $\boldsymbol{G_{E_d}}(p)$, $\boldsymbol{G_{E_q}}(p)$ and $\boldsymbol{G_s}(p)$ in (8) become $\boldsymbol{G_{E_d\_E_d}}(p)$, $\boldsymbol{G_{E_q\_E_q}}(p)$ and $\boldsymbol{G_{s\_sE_d}}(p)$ in (9), and Fig. 3 becomes Fig. 4.

2) Reduction of dynamics of $\Delta \boldsymbol{X_c}$ and Δs (constant $\boldsymbol{X_c}$ and s model)

The third-order model shown in (14) and Fig. 4 is the most commonly used simplified model of DFIGs in the existing research. By applying the modeling adequacy assessment, it has been discovered in this paper that the third-order model can be further reduced. When the participation level of both $\Delta \boldsymbol{X_c}$ and Δs is below certain threshold, the dynamics of $\Delta \boldsymbol{X_c}$ and Δs can be neglected at the same time and the linearised dynamic model becomes (15) and is displayed in Fig. 5. The electric torque is considered to be equal to the mechanical torque in this model so that the rotor speed could stay constant.

$$\begin{bmatrix} \Delta \dot{E}_d \\ \Delta \dot{E}_q \end{bmatrix} = \begin{bmatrix} A_{22w} & 0 \\ 0 & A_{33w} \end{bmatrix} \begin{bmatrix} \Delta E_d \\ \Delta E_q \end{bmatrix} + \begin{bmatrix} \boldsymbol{B_{2w}} \\ \boldsymbol{B_{3w}} \end{bmatrix} \Delta \boldsymbol{V_w} \tag{15}$$

3) Reduction of dynamics of $\Delta \boldsymbol{X_c}, \Delta E_d$ and ΔE_q (constant $\boldsymbol{X_c}$ and $\Delta \dot{E}_{d/q} = 0$ model)

On the basis of the model reduction presented in 1), the dynamics of rotor flux represented by ΔE_d and ΔE_q can be further neglected by setting $\Delta \dot{E}_d = 0$ and $\Delta \dot{E}_q = 0$ in small-signal rotor angle stability analysis [30]. Due to the existence of offset voltage items in RSC controller, the physical meaning of $\Delta \dot{E}_d = 0$ and $\Delta \dot{E}_q = 0$ is that the dynamics of inner current loop of RSC controller is ignored and the rotor current can track its reference instantaneously. This reduction is usually considered to be reasonable in small-signal rotor angle stability analysis as the inner current loop responses much faster than the electromechanical transient [30]. As a result, ΔE_d and ΔE_q become algebraic variables like terminal voltage and the dynamic model associated with ΔE_d and ΔE_q in (14) becomes algebraic model. The linearised dynamic model after the reduction of dynamics of $\Delta \boldsymbol{X_c}, \Delta E_d$ and ΔE_q is shown in Fig. 6.

According to Fig. 6, it is straight forward to assess the impact of the reduction of rotor flux dynamics on the critical eigenvalue by simply setting $p = 0$ for $(p\boldsymbol{I} - \boldsymbol{A_{22w}})^{-1}$ and $(p\boldsymbol{I} - \boldsymbol{A_{33w}})^{-1}$ in (8) and (9). It can be concluded that further reductions on the dynamics of ΔE_d and ΔE_q could be carried out if the change in the participation level of ΔE_d and ΔE_q (before and after $p = 0$) is less than the preset threshold.

4) Reduction of dynamics of $\Delta \boldsymbol{X_c}, \Delta s, \Delta E_d$ and ΔE_q (constant $\boldsymbol{X_c}$, s and $\Delta \dot{E}_{d/q} = 0$ model)

Similarly, if the requirement of dynamics reduction in 2) and 3) are met simultaneously, the model reductions can be combined together, and hence the dynamic model of the DFIG becomes a pure algebraic model without differential equations. That is to say, the introduction of constant $\boldsymbol{X_c}$, s and $\Delta \dot{E}_{d/q} = 0$ model of DFIGs to the system would not increase the computational burden. Similar to Step 3), this model can be easily derived from the constant

$\mathbf{X_c}$ and s model in Fig. 5 by setting $p = 0$.

5) Reduction of dynamics of $\Delta \boldsymbol{X_c}, \Delta s, \Delta E_d$ and ΔE_q (constant $\boldsymbol{X_c}$, s and $E_{d/q}$ model)

If the participation level of all the state variables of the DFIG in affecting the critical eigenvalue is very low, all dynamics of the DFIG can be removed in the study. In this case, as demonstrated by (4), the DFIG can be modeled as a constant admittance with constant $\mathbf{X_c}$, s, E_d and E_q.

The generator-level model reduction plans proposed above are summarized in Table 1 so as to differentiate these reduced models and reveal their physical insight and potential applications.

3.2 Model Reduction Strategy for a Power System with Multiple Doubly-fed Induction Generators (System Level)

The model reduction plans in the previous subsection provide different reduction possibilities for the DFIG internal dynamic model. On this basis, a model reduction strategy is proposed for grid-connected DFIGs on the multi-machine system level, with the aim to reduce the complexity of system dynamic model as a whole for small-signal rotor angle stability analysis. Therefore, the model reduction should start from the dynamic model of DFIGs with comparatively low level of the participation. For instance, some small-scale DFIG-based wind farms are located far away from main-interconnected system, the dynamics of which might have a very limited impact on the critical eigenvalue and could be generally ignored by model reduction plans (i.e., Model 4) and 5)). A concept of model reduction margin (MRM) is proposed to be a predetermined threshold to measure if the computed participation level is high or low and define the maximal real part variation of the critical eigenvalues (either +ve or -ve) allowed in the model reduction. Since most of time the damping performance of the oscillation is described by the damping ratio, a relationship between MRM and the allowed variation of damping ratio ζ of the critical eigenvalue $\lambda_i = \sigma + j\omega$ is presented as follows

$$\mathrm{MRM} = \left| \frac{\mathrm{a}\%\omega}{\sqrt{1-(\mathrm{a}\%)^2}} \right| \tag{16}$$

where a% is the allowed variation of damping ratio ζ (e.g., if a% is set to 0.02% and $\zeta = 3\%$, it means the variation range allowed for ζ is from 2.98% to 3.02%). There is no strict rule to set the value of a% for the model reduction and it could vary with different system requirements or grid codes. A proper a% can maximize the acceptable MRM and hence reduce more model orders without significantly affecting the model accuracy. In practice, a trial and error method can be used to compare the simulation curves to see any significant errors between the plots and determine the value of a%. Normally, an empirical value of a% equal to 0.02% can be an ideal starting point. The detailed steps of the model reduction strategy can be demonstrated as follows:

1. a% is set up and MRM is calculated according to (16).
2. DFIGs are ranked based on their respective participation level (total contribution to the critical eigenvalue) from low to high in affecting system damping, by using the results from the proposed modeling adequacy assessment.
3. The dynamic model reduction starts from the DFIGs with the lowest participation level to the ones with higher participation level. The DFIG with lower participation level will have a higher priority for model reduction. For each DFIG, five model reduction plans

are provided for selection (on generator level). The more reduced models (e.g., Model 5)) have the higher priority to be chosen if the accumulative participation level (real part variation of the critical eigenvalue) does not breach MRM. The feasibility of less reduced models will be checked if the more reduced models are not qualified. The model reduction continues on every ranked DFIG as long as the accumulative eigenvalue variation is still within MRM.

4. The model reduction stops when MRM is reached to its predetermined threshold. Upon this step the most effective model reduction strategy for the entire dynamic system (on system level) is finalized.

4. CASE STUDY

4.1 Case 1: Model Reduction of New England Test System

The New England test system illustrated in Fig. 7 is used to demonstrate the proposed method of modeling adequacy assessment and the model reduction strategy. This test system represents a reduced system model of the transmission power grid in New England region (i.e., six states in the Northeastern US). It is a standard test system used by numerous researchers to study both static and dynamic problems in the power system. As shown in Fig. 7, the system consists of three areas. In Area 1, there are 2230 MW of generation and 2380 MW of load; In Area 2, there are 790 MW of generation and 1120 MW of load; In Area 3, there are 3180 MW of generation and 2650 MW of load. The system has 10 SGs, 39 buses, 19 loads, 34 transmission lines and 12 transformers in total. All of the SGs are equipped with an IEEE type-1 exciter and a simple turbine governor, except SG10 which is an equivalent generator representing the New York power system and is considered not to have a governor. The parameters of the network and SGs are available in [31]. A detailed twelfth-order DFIG model consisting of third-order induction generator ($\Delta s, \Delta E_d$ and ΔE_q), fourth-order RSC controller, fourth-order GSC controller and first-order DC link (i.e., $\Delta \boldsymbol{X_{c9\times 1}}$) is employed as a benchmark model for the model reduction in this case, which is presented with its parameters in Appendix A.3. Three DFIG-based wind farms (WF1-3) are connected to the test system at bus 19, 30 and 36. The active power output and terminal voltage of the three DFIGs are also given in Appendix A.3.

In this case, the 17th eigenvalue λ_{17} is regarded as the critical eigenvalue as an example for demonstration purposes. The critical eigenvalue reflects the inter-area oscillation mode between the New England test system (SGs 1-9) and external New York power system (represented by the equivalent generator SG10), with the oscillation frequency around 0.5Hz. The impact of DFIGs on the critical eigenvalue includes two parts: the constant admittance of DFIGs, and the dynamic model components of DFIGs. The critical eigenvalue considering the impact of the constant admittance is denoted as λ_{17}^{CA}, and calculated by state matrix in (4) or (5), $\lambda_{17}^{CA} = -0.1199 + j3.2452$. The impact of dynamic model components on the critical eigenvalue is denoted as $\Delta\lambda_{17}$, which is calculated by (13) in modeling adequacy assessment, and presented in Table 2. The real part of the eigenvalue contribution in Table 2 indicates the participation of each dynamic model component of the DFIGs in affecting the system damping performance. It can be revealed that different connecting locations lead to different eigenvalue contributions to system dynamics. According to (13), the eigenvalue contribution from the dynamics of all DFIGs in Table 2 is summed up, i.e., $\Delta\lambda_{17} = \Delta\lambda_{17}(WF1) + \Delta\lambda_{17}(WF2) + \Delta\lambda_{17}(WF3) = 0.0438 - j0.1012$. Finally, the critical eigenvalue considering the impact of the constant admittance and dynamic components of the DFIGs can be estimated

to be

$$\lambda_{17}^{CA} + \Delta\lambda_{17} = -0.0761 + j3.1440 \quad (17)$$

To validate the method above, modal analysis is carried out to calculate critical eigenvalue (λ_{17}^{MA}) based on detailed dynamic model of the test system with no reduction on any DFIG model. The result can be obtained

$$\lambda_{17}^{MA} = -0.0760 + j3.1448 \quad (18)$$

By comparing the results of (17) and (18), the accuracy of the proposed modeling adequacy assessment method can be verified.

On the basis of the above modeling adequacy assessment, the model reduction strategy is adopted for the dynamic model reduction of the three DFIGs.

According to the detailed procedure presented in Subsection 3.2, MRM is firstly calculated

$$\text{MRM} = 6.2896 \times 10^{-4} \quad (19)$$

where the critical eigenvalue is equal to λ_{17}^{MA} and a% is set to 0.02%. Then the DFIGs are ranked as WF2, WF3 and WF1 according to the real part of total eigenvalue contributions from each DFIG as shown in Table 2, which are 0.0111, 0.0131 and 0.0196 respectively. The less the eigenvalue contribution is, the lower the participation level is. Hence, the dynamic model reduction starts from the least important WF2 which has the lowest participation level. By comparing with MRM, model reduction plan 4) is selected for WF2, and model reduction plan 2) for WF1. The detailed dynamic model of WF3 should be retained as the further reduction of $\Delta \boldsymbol{X_c}$ dynamics will breach MRM in this case. After the model reduction, the total eigenvalue (real part) variation is -5.6394×10^{-4}, and thus the estimated critical eigenvalue is $-0.0766 + j3.1459$.

To validate the model reduction strategy, time-domain simulation based on different DFIG dynamic models is implemented. MATLAB is employed for the time-domain electromechanical simulation with different WF dynamic models and the simulation time span is set for 10 seconds. A three-phase short-circuit fault is applied to Bus 1 for $0.1s$. SG5, SG9 and SG10 are the major generators associated with this critical oscillation mode and hence the power angle difference between SG5 and SG10 and power angle difference between SG9 and SG10 are plotted in Fig. 8.1 and Fig. 8.2. It can be seen from Fig. 8.1 and Fig. 8.2 that there is no significant difference between the application of the detailed DFIG models and reduced DFIG models. Therefore the model reduction strategy could retain the accuracy of dynamic study, and the simulation results are consistent with the results in frequency domain.

The simulation time and dynamic model complexity (in term of order) before and after the model reduction is compared in Table 3. The same computational resource (Lenovo ThinkCentre, Intel Core i7-4790 CPUs 3.60 GHz, 32.0 GB RAM) is employed. Around 25% of total simulation time is saved after adopting the reduced DFIG models. It will be demonstrated by the next case that time saving would be more considerable with a larger number of DFIGs connected.

Therefore, by taking account of both accuracy and efficiency, the benefits of the proposed model reduction strategy have been demonstrated.

4.2 Case 2: Model Reduction of JS Power Grid in Eastern China

A case study of a real provincial power grid is presented in Case 2. JS power grid is a real power grid in Jiangsu Province, Eastern China, which covers 13 cities and 51 towns. The configuration of the grid is displayed in Fig. 9. There are totally 53 SGs, 13 DFIG-based wind farms, 1713 buses and 2771 transmission lines in the grid, with 110 GW installing generation capacity (5.6 GW from wind power generation). JS power grid is interconnected with four external grids in Eastern China including AHG, ZJG, SHG and YCG as shown. The load center of JS power grid is located in the South River Land (e.g., NJN, CZN, WXN and SZN), which is however supplied by big power plants in the North River Land (e.g., XZN, LYGN, YCN and TZN). Bulk power generated in the north is transmitted via the long transmission lines across Yangtze River to the south, which is a typical scenario where stability problem might occur. More precisely, there is an inter-area oscillation mode (or named SB oscillation mode) inside JS power grid between northern and southern regions, with the oscillation frequency around 0.64Hz. 13 DFIG-based wind farms are installed along the east coast areas where the wind resource is abundant. Due to the factors such as different locations and installed capacities, WFs have different impacts on the SB oscillation mode and hence can have different modeling complexities in the small-signal rotor angle stability analysis, which deserves a careful investigation for a computational resource-limited environment of system operation.

The critical eigenvalue of the SB oscillation mode is calculated as $-0.1906 + j4.0337$ and if a% is set to 0.03%, $\mathrm{MRM} = 0.0012$. Then by assessing the modeling adequacy and applying the model reduction strategy, the reduced dynamic models of the 13 wind farms can be determined and shown in Table 4. It can be revealed from Table 4 that: 1. GYW is located close to TWSG (the SG with the highest participation factor of the SB oscillation mode) and its dynamics have a big impact on the system damping. Thus, GYW should be modeled in details with no reduction; 2. Most wind farms connected to YCN are close to the major transmission network, which can interact with the power oscillation effectively, and hence should reduce only one or two dynamic components with comparatively detailed dynamic models (e.g., Model 1) and 2)); 3. The small-scale wind farms connected to NTN are located far away from the main-interconnected system and therefore less involved in the power system oscillation. As a result, the most simplified dynamic models (e.g., Model 4) and 5)) are employed for those WFs.

MATLAB is employed for the time-domain electromechanical simulation with different WF dynamic models and the simulation time span is set for 10 seconds. The results of time-domain simulation with both reduced WF dynamic models and detailed models are shown in Fig. 10.1 and Fig. 10.2. A three-phase short-circuit fault is applied to Bus 1114 for $0.1s$. TWSG (LYGN), PCSG (XZN), HSSG (SZN) and LRSG (NJN) are the major generators associated with this inter-area oscillation mode and hence are observed. Table 5 provides the comparison results of the computational time and modeling complexity before and after the model reduction. Each of 53 SGs adopts 8-order model and each of 13 DFIGs adopts 12-order model before the reduction and thus the total model complexity of the system is 580^{th} order when using the detailed DFIG model.

Based on the comparison in Fig. 10.1, Fig. 10.2 and Table 5, it can be proved that the reduced model is accurate enough to replace the detailed model for small-signal rotor angle stability analysis in a real power grid operation environment, and the advantage of the proposed model reduction strategy is to improve the computational efficiency by 28.5% for the time-consuming dynamic study.

5. DISCUSSIONS ON PRACTICAL APPLICATIONS

Compared with the connecting location and design parameters of DFIGs, the impact of system outage plans and DFIG operating conditions on the damping contributions of DFIG dynamics is minor according to the operational experience. Therefore, once the DFIGs are connected into the system (i.e., installing location and design parameters are determined), the model reduction strategy of DFIGs can be implemented based on the generation patterns, demand forecasting and network outages (on the critical stability path) of the planning days. Two typical applications of the dynamic model reduction in improving the computational efficiency of system operation and planning are given as follows:

1. In the real-time operation environment, since the wind forecasting is not quite reliable, the impact of different operating conditions of DFIGs on the system critical oscillation mode is regularly analysed by electricity system operator, in order to identify any dispatch requirement on generators to improve the small-signal rotor angle stability margin. For example, the on-line stability assessment runs shortly and repeatedly by taking the snapshot of real operating systems. The DFIG model reduction plans can be adopted into such stability assessment during different wind speed conditions, to improve the computational efficiency, and save time for electricity system operator to take actions against potential stability issues. Since the changing wind speed mainly affects the wind output power and hence the constant admittance of DFIGs rather than the damping contribution of DFIG dynamics [32], the same DFIG model reduction plans can be used for different wind speed conditions.

2. In the power system planning environment, to assess numerous network outage plans from several years ahead to day ahead, both small-signal and transient stability need to be taken into account for typical inter-area stability constraint (e.g., Scottish export stability constraint (SCOTEX) in Great Britain power system). The model reduction strategy of DFIGs could be applied to aid the efficiency of dynamic study for various network outage plans. It is worth mentioning for majority of outage plans that are not on the critical stability path, model reduction strategy only needs to be carried out once to further reduce the computational time for time-domain stability simulations.

It is also worthy to mention that the same model reduction plan might not suit all the inter-area oscillation modes between different areas of the system at the same time and therefore multiple model reduction plans could be produced by the proposed strategy for the most critical and major system oscillation modes with time-consuming assessments respectively (e.g., SCOTEX and NKILGRMO oscillation modes for GB transmission system, and SB and YC oscillation modes for JS power grid), which is certainly beneficial for the efficiency improvement of system planning on comprehensive study points of the planning period. It can be foreseen that the proposed model reduction strategy will particularly benefit the pressed day-ahead planning with massive scenarios to assess, and more resources will be saved if more system planners implement the strategy on different planning stages.

6. CONCLUSIONS

This paper presents a novel method to reduce the model complexity of doubly-fed induction generator-based wind generation for power system small-signal rotor angle stability analysis. Model reduction strategy is achieved by the following steps:

1. In the model adequacy assessment, the participation levels of each component of doubly-fed induction generators in affecting system damping are assessed.

2. Sum up the participation level of dynamic components of doubly-fed induction generators to obtain total participation level for all doubly-fed induction generators. Doubly-fed induction generators with lower participation level contribute less to system damping, and therefore will be simplified first.
3. Five dynamic model reduction schemes of doubly-fed induction generators are provided for selections in order to reduce the model complexity of doubly-fed induction generators to desired levels, based on the calculated participation level.
4. Model reduction strategy stops when model reduction margin is reached.

The above model reduction strategy has been implemented for dynamic study of the New England test system, and JS power grid in China respectively. Two practical applications are discussed in the power system operation and planning environments. It has been demonstrated that the proposed model reduction strategy of doubly-fed induction generators will improve the calculation efficiency of power system dynamic study, while still maintain the study accuracy to an acceptable level.

ACKNOWLEDGMENT

The authors would like to acknowledge the support from Department of Electrical Engineering, The Hong Kong Polytechnic University for the Start-up Fund Research Project (1-ZE68), Research Grant Council (HK) for the Early Career Scheme Grant Research Project (25203917), Beijing Natural Science Foundation (3174057), and Support Program for the Excellent Talents in Beijing City (2016000020124G079).

APPENDIX

A.1 Derivation of $\boldsymbol{\gamma_{ik}}$

According to the algebraic equation of (3), it can obtain

$$\Delta \boldsymbol{V_w} = \boldsymbol{C_{V_w X_g}} \Delta \boldsymbol{X_g} \tag{A1}$$

If λ_i and $\boldsymbol{v_i}$ is the i^{th} eigenvalue and associated right eigenvector of state matrix $\left(\boldsymbol{A_g} - [\boldsymbol{BD^{-1}C}]_{\boldsymbol{g}}\right)$ in (4), it can have

$$\Delta \boldsymbol{X_g} = \sum_{i=1}^{n} \frac{\boldsymbol{v_{ig}} a_i}{p-\lambda_i}, \Delta\omega_k = \sum_{i=1}^{n} \frac{v_{ik} a_i}{p-\lambda_i} \tag{A2}$$

where $\boldsymbol{v_{ig}}$ is the vector inside $\boldsymbol{v_i}$ corresponding to $\Delta \boldsymbol{X_g}$, and v_{ik} is the element of $\boldsymbol{v_i}$ corresponding to $\Delta\omega_k$. Based on (A1) and (A2), the relationship between $\Delta \boldsymbol{V_w}$ and $\Delta\omega_k$ can be derived.

$$\Delta \boldsymbol{V_w} = \boldsymbol{C_{V_w X_g}} \left(\sum_{i=1}^{n} \frac{\boldsymbol{v_{ig}} a_i}{p-\lambda_i} \Big/ \sum_{i=1}^{n} \frac{v_{ik} a_i}{p-\lambda_i} \right) \Delta\omega_k = \boldsymbol{\gamma_{ik}} \Delta\omega_k \tag{A3}$$

A.2 Derivation of $\boldsymbol{S_{ik}}$

The sensitivity of λ_i with respect to the electric torque coefficient of the k^{th} SG can be computed to be

$$S_{ik} = \frac{\partial \lambda_i}{\partial TC_{wk}} = w_{ik} v_{ik} \quad \text{(A4)}$$

where w_{ik} is the element of λ_i associated left eigenvector $\boldsymbol{w_i}$ corresponding to $\Delta\omega_k$.

A.3 DFIG Models and Parameters

A.3.1 Induction Generator Parameters

$S_{DFIG} = 70MVA, M_w = 3.4s, D_w = 0, R_r = 0.0007, X_s = 0.0878, X_r = 0.0373, X_m = 1.3246, X_{r3} = 0.05, V_{dc0} = 1, C_{GSC} = 13.29$

A.3.2 Converter Control System Models and Parameters

RSC controller parameters: (Fig. 11(a))

$K_{psp1} = K_{qsp1} = 0.2, K_{psp2} = K_{qsp2} = 1, K_{psI1} = K_{qsI1} = 12.56s^{-1}, K_{psI2} = K_{qsI2} = 62.5s^{-1}$

GSC controller parameters: (Fig. 11(b))

$K_{vdcp1} = K_{qr3p1} = 0.2, K_{vdcp2} = K_{qr3p2} = 1, K_{vdcI1} = K_{qr3I1} = 12.56s^{-1}, K_{vdcI2} = K_{qr3I2} = 62.5s^{-1}$

A.3.3 Operational Conditions

$P_{w1} = P_{w2} = P_{w3} = 2.0\ p.u., V_{w1} = V_{w2} = V_{w3} = 1.025\ p.u.$

REFERENCES

[1] Chen H, Wang C, Cai W, Wang J. Simulating the impact of investment preference on low-carbon transition in power sector, Applied Energy 2018; 217:440-55.

[2] Wang L, Wei Y, Brown M. Global transition to low-carbon electricity: A bibliometric analysis, Applied Energy 2017; 205:57-68.

[3] Wang C, Yan J, Marnay C, Djilali N, Dahlquist E, Wu J, Jia H. Distributed Energy and Microgrids (DEM). Applied Energy 2018; 210:685-89.

[4] McKenna R, Djapic P, Weinand J, Fichtner W, Strbac G. Assessing the implications of socioeconomic diversity for low carbon technology uptake in electrical distribution networks. Applied Energy 2018; 210:856-69.

[5] Wang M, Mu Y, Jia H, Wu J, Yu X, Qi Y. Active power regulation for large-scale wind farms through an efficient power plant model of electric vehicles. Applied Energy 2017; 185:1673-83.

[6] Zhang X, Ma C, Song X, Zhou Y, Chen W. The impacts of wind technology advancement on future global energy, Applied Energy 2016; 184:1033-37.

[7] Kumar Y, Ringenberg J, Shekara Depuru SS, Devabhaktuni VK, Lee JW, Nikolaidis E, Andersen B, Afjeh A. Wind energy: Trends and enabling technologies. Renewable and Sustainable Energy Reviews 2016; 53:209-24.

[8] Global Wind Statistics; 2016. <http://www.gwec.net/wp-content/uploads/vip/GWEC_PRstats2016_EN_WEB.pdf> [accessed 10.02.17].

[9] Xie D., Lu Y. P., Sun J. B., Gu C. H.. Small signal stability analysis for different types of PMSGs connected to the grid. Renewable Energy, 2017; 106:149-164.

[10] Modi N, Saha TK, Anderson T. Damping performance of the large scale Queensland transmission network with significant wind penetration. Applied Energy 2013; 111:225-33.
[11] Song Z, Xia C, Shi T. Assessing transient response of DFIG based wind turbines during voltage dips regarding main flux saturation and rotor deep-bar effect. Applied Energy 2010; 87:3283-93.
[12] Yang B, Yu T, Shu H, Dong J, Jiang L. Robust sliding-mode control of wind energy conversion systems for optimal power extraction via nonlinear perturbation observers. Applied Energy 2018; 210:711-23.
[13] Slootweg J, Polinder H, Kling W. Dynamic Modeling of a Wind Turbine with Doubly Fed Induction Generator. Power Engineering Society Summer Meeting, Vancouver, BC, Canada, 2001; 1:644-49.
[14] Ekanayake J, Holdsworth L, Wu X, Jenkins N. Dynamic Modeling of Doubly Fed Induction Generator Wind Turbines. IEEE Trans. Power Systems, 2003; 2:803-809.
[15] Pal B, Mei F. Modeling Adequacy of the Doubly-fed Induction Generator for Small-signal Stability Studies in Power Systems. IET Renewable Power Generation, 2008; 3:181-190.
[16] Wu F, Zhang X, Godfrey K, Ju P. Modeling and Control of Wind Turbine with Doubly Fed Induction Generator. Power Systems Conference and Exposition, 2006; 1404-1409.
[17] Hughes F, Anaya-Lara O, Jenkins N, Strbac G. Control of DFIG-Based Wind Generation for Power Network Support. IEEE Trans. Power Systems, 2005; 4:1958-1966.
[18] Xi X, Geng H, Yang G. Enhanced model of the doubly fed induction generator-based wind farm for small-signal stability studies of weak power system. IET Renewable Power Generation, 2014; 7:765-774.
[19] Ekanayake J, Holdsworth L, Jenkins N. Comparison of 5th order and 3rd order machine models for doubly fed induction generator (DFIG) wind turbines. Electric Power Systems Research, 2003; 3:207-215.
[20] Feijoo A, Cidras J, Carrillo C. A third order model for the doubly-fed induction machine. Electric Power Systems Research, 2000; 2:121-127.
[21] Elkington K, Knazkins V, Ghandhari M. On the stability of power systems containing doubly fed induction generator-based generation. Electric Power Systems Research, 2008; 9:1477-1484.
[22] Pulgar-Painemal H, Sauer P. Reduced-order model of type-c wind turbine generators. Electric Power Systems Research, 2011; 4:840-845.
[23] Ghosh S, Senroy N. Balanced truncation based reduced order modeling of wind farm. International Journal of Electric Power & Energy Systems, 2013; 53:649-655.
[24] Pulgar-Painemal H, Sauer P. Towards a wind farm reduced-order model. Electric Power Systems Research, 2011; 8:1688-1695.
[25] Ni Y, Li C, Du Z, Zhang G. Model order reduction based dynamic equivalence of a wind farm. International Journal of Electric Power & Energy Systems, 2016; 83:96-103.
[26] Wang X, Song Y, Irving M. Modern Power Systems Analysis. Berlin, Gernany: Springer, 2011.
[27] Du W, Bi J, Cao J, Wang H. A Method to Examine the Impact of Grid Connection of the DFIGs on Power System Electromechanical Oscillation Modes. IEEE Trans. Power Systems, 2016; 5:3775-3785.
[28] Mei F, Pal B. Modal Analysis of a Grid-Connected Doubly Fed Induction Generator. IEEE Trans. Energy Conversion, 2007; 3:728-736.
[29] Ledesma P, Usaola J. Effect of neglecting stator transients in doubly fed induction generators models. IEEE Trans. Energy Conversion, 2004; 2:459-461.

[30] Ellis A, Kazachkov Y, Muljadi E, Pourbeik P, Sanchez-Gasca J. Description and Technical Specifications for Generic WTG Models – A Status Report. IEEE PES Power Systems Conference and Exposition (PSCE) 2011; 1-8.
[31] Rogers G. Power System Oscillations. Norwell, MA, USA: Kluwer, 2000.
[32] Bu S, Zhang X, Zhu J, Liu X. Comparison analysis on damping mechanisms of power systems with induction generator based wind power generation. International Journal of Electrical Power and Energy Systems, 2018; 97:250-261.

List of Tables:

Table 1 A Summary of Proposed Generator-level Model Reduction Plans

Reduction Plan No.	Reduced Model	Physical Insight and Potential Applications
1)	Constant $\boldsymbol{X_c}$ Model	Applied when dynamic impact of RSC/GSC integral controller and DC link on the eigenvalues can be negligible.
2)	Constant $\boldsymbol{X_c}$ and s Model	Applied when the requirement of 1) is met and also the assumption of constant rotor speed (mechanical and electric torque balance) has a minor impact on the eigenvalues.
3)	Constant $\boldsymbol{X_c}$ and $\Delta\dot{E}_{d/q} = 0$ Model	Applied when the requirement of 1) is met and also the dynamics of inner current loop of RSC controller can be ignored, which means the rotor current can track its reference instantaneously.
4)	Constant $\boldsymbol{X_c}$, s and $\Delta\dot{E}_{d/q} = 0$ Model	Applied when the requirements of 1) 2) 3) are met.
5)	Constant $\boldsymbol{X_c}$, s and $E_{d/q}$ Model	Applied when the dynamic interactions between DFIGs and SGs can be ignored and DFIGs are only modeled as a constant admittance/impedance determined by their algebraic interface equations.

Table 2 Participation Level (Eigenvalue Contributions) from Different DFIG Dynamics

$\Delta\lambda_{17}$	From WF1	From WF2	From WF3
Δs	$-8.2633 \times 10^{-5} + j1.1072 \times 10^{-5}$	$-1.5575 \times 10^{-5} - j1.0050 \times 10^{-5}$	$-5.2153 \times 10^{-5} - j1.6774 \times 10^{-5}$
ΔE_d	$-8.9922 \times 10^{-5} - j4.0514 \times 10^{-4}$	$4.5767 \times 10^{-5} - j8.7290 \times 10^{-5}$	$6.2514 \times 10^{-5} - j2.7911 \times 10^{-4}$
ΔE_q	$0.0192 - j0.0733$	$0.0109 - j0.0072$	$0.0128 - j0.0180$
$\Delta \boldsymbol{X_c}$	$0.0005 - j0.0014$	$2.2901 \times 10^{-4} - j1.2328 \times 10^{-4}$	$2.8821 \times 10^{-4} - j3.3864 \times 10^{-4}$
Total	$0.0196 - j0.0751$	$0.0111 - j0.0074$	$0.0131 - j0.0187$

Table 3 Computational Time of Simulation before and after Model Reduction (New England Test System)

Before Reduction (76^{th}-order Model)	After Reduction (54^{th}-order Model)
93.28*s*	75.32*s*

Table 4 Model Reduction Plan for 13 Wind Farms in JS Power Grid

Wind Farm	Location	Model Reduction Plan
DFW	YCN	Model 1)
BHW	YCN	Model 1)
SYW	YCN	Model 1)
DTW	YCN	Model 2)
GHW	YCN	Model 1)
XSW	YCN	Model 1)
GYW	LYGN	Detailed Model
LHW	NTN	Model 5)
DLW	NTN	Model 4)
LYW	NTN	Model 2)
DYW	NTN	Model 4)
RDW	NTN	Model 4)
HQW	NTN	Model 4)

Table 5 Computational Time of Simulation before and after Model Reduction (JS Power Grid)

Before Reduction (580^{th}-order Model)	After Reduction (456^{th}-order Model)
751.47*s*	537.25*s*

List of Figures:

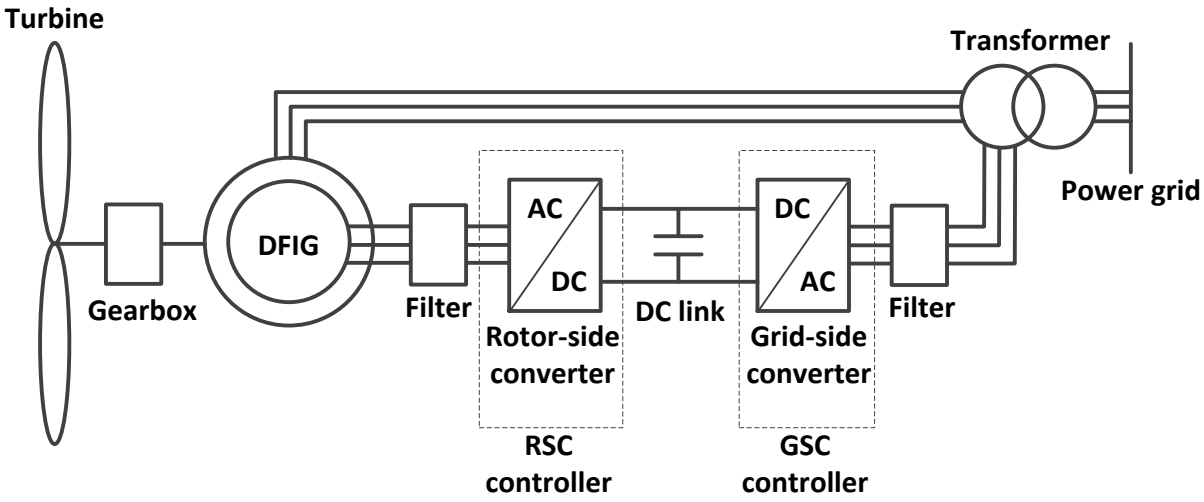

Fig. 1 Schematic diagram of a DFIG-based wind generation

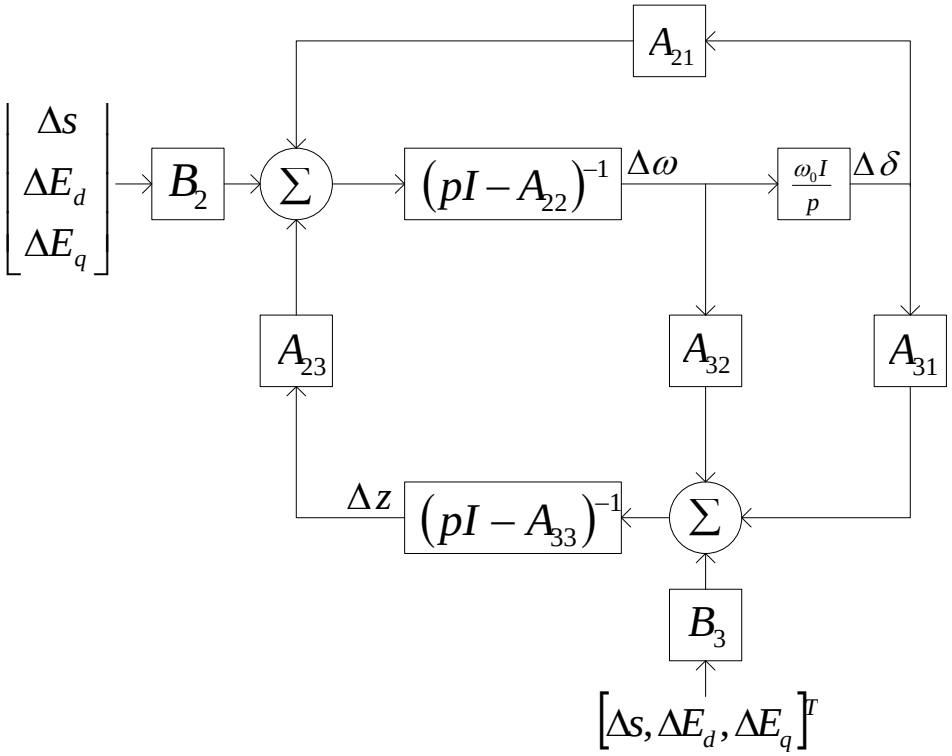

Fig. 2 Linearised model of power system integrated with DFIGs (System-part Dynamics)

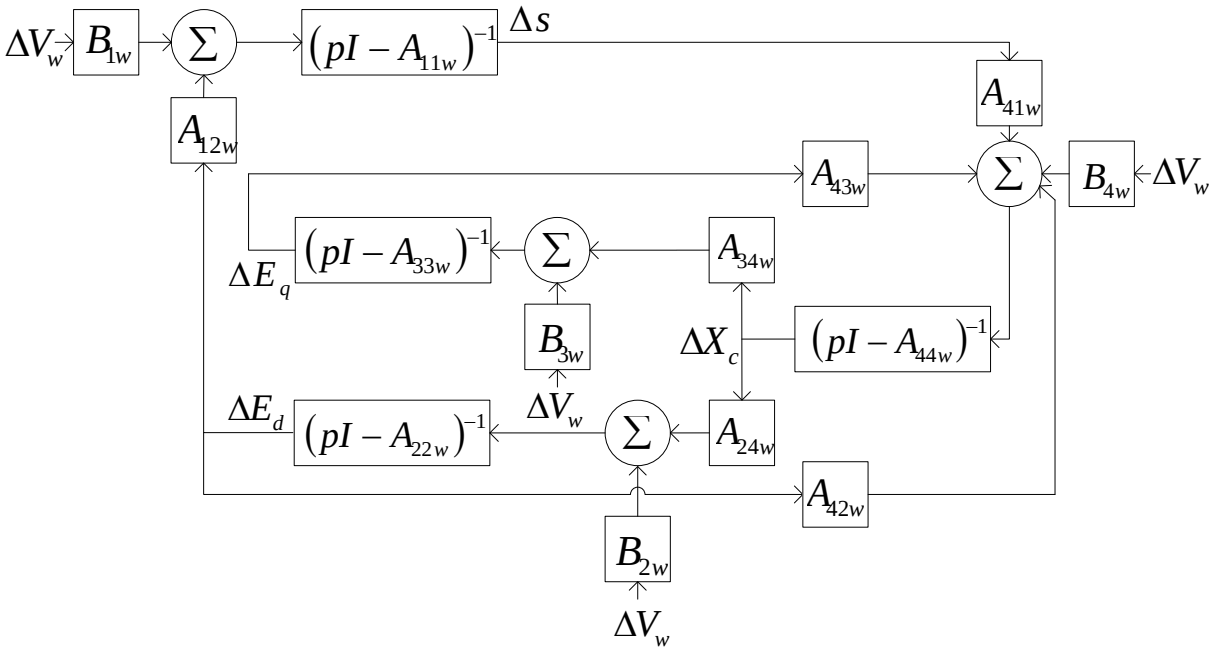

Fig. 3 Linearised model of DFIG internal dynamics (DFIG-part Dynamics)

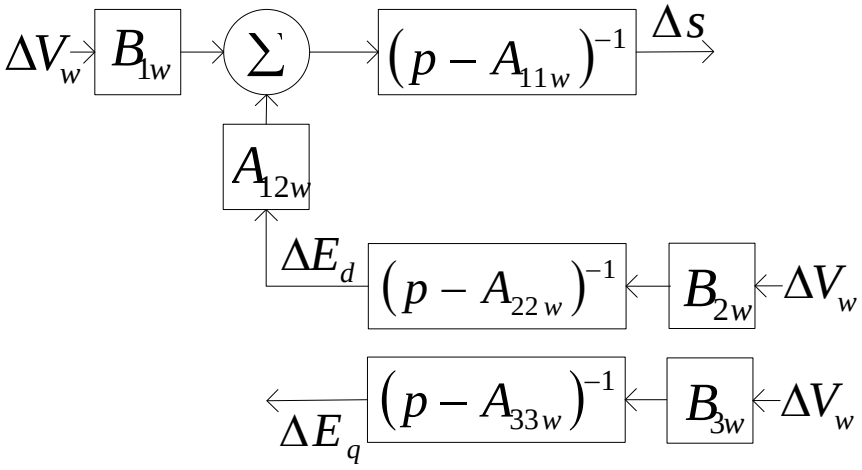

Fig. 4 Constant $\boldsymbol{X_c}$ model of DFIG internal dynamics

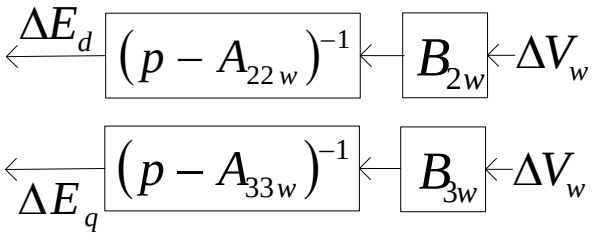

Fig. 5 Constant $\boldsymbol{X_c}$ and Δs model of DFIG internal dynamics

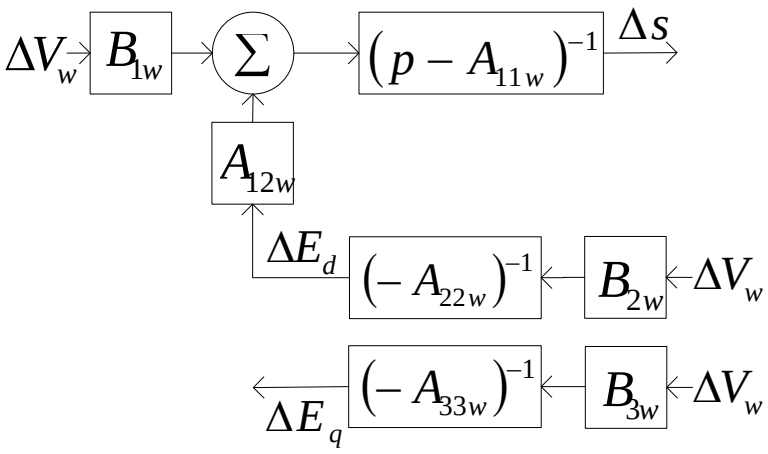

Fig. 6 Constant $\boldsymbol{X_c}$ and $\Delta\dot{E} = 0$ model of DFIG internal dynamics

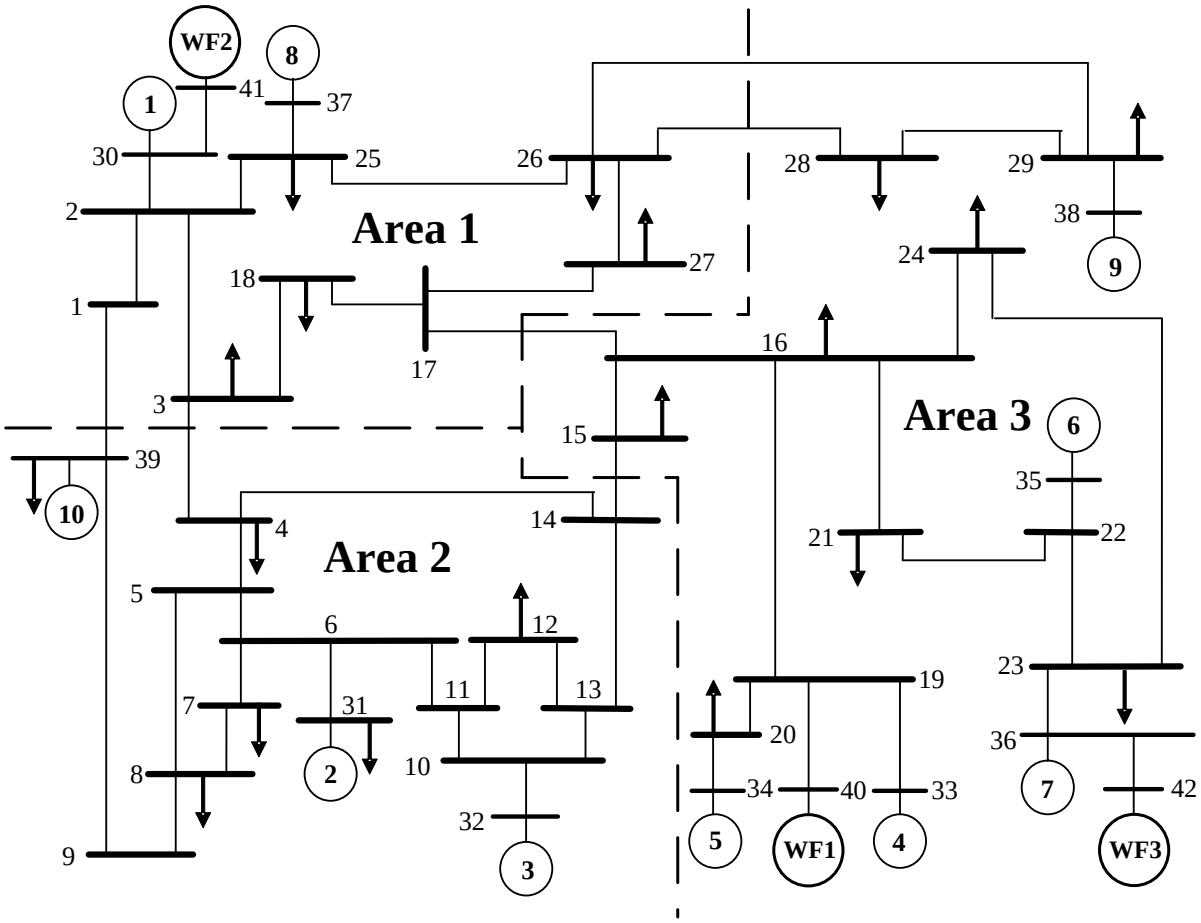

Fig. 7 Line diagram of 10-machine 39-bus New England test system integrated with 3 DFIG-based WFs

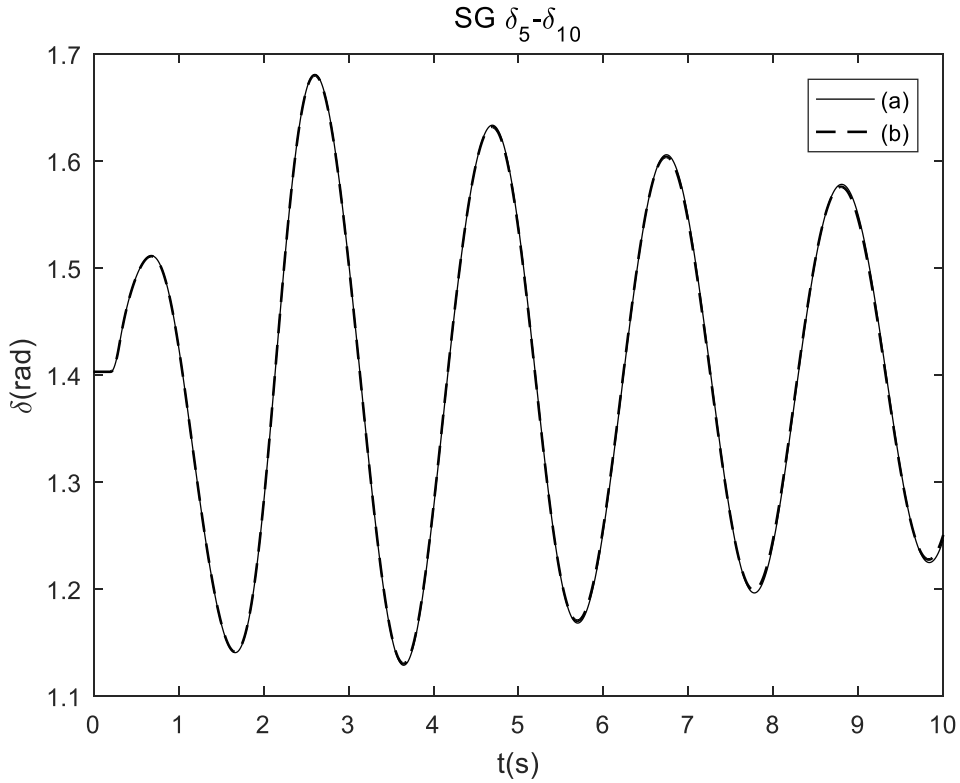

Fig. 8.1 SG5-SG10 power angle difference with different WF dynamic models
(a) Three WFs with detailed model (benchmark); (b) WF1 with reduced model 2), WF2 with reduced model 4) and WF3 with detailed model

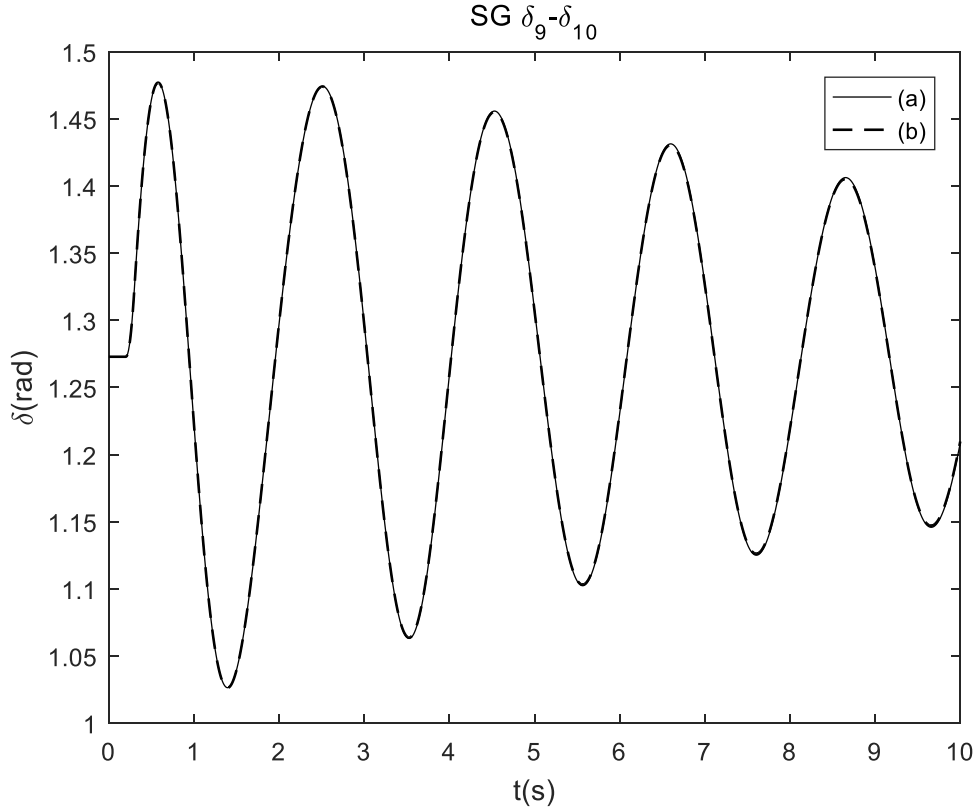

Fig. 8.2 SG9-SG10 power angle difference with different WF dynamic models
(a) Three WFs with detailed model (benchmark); (b) WF1 with reduced model 2), WF2 with reduced model 4) and WF3 with detailed model

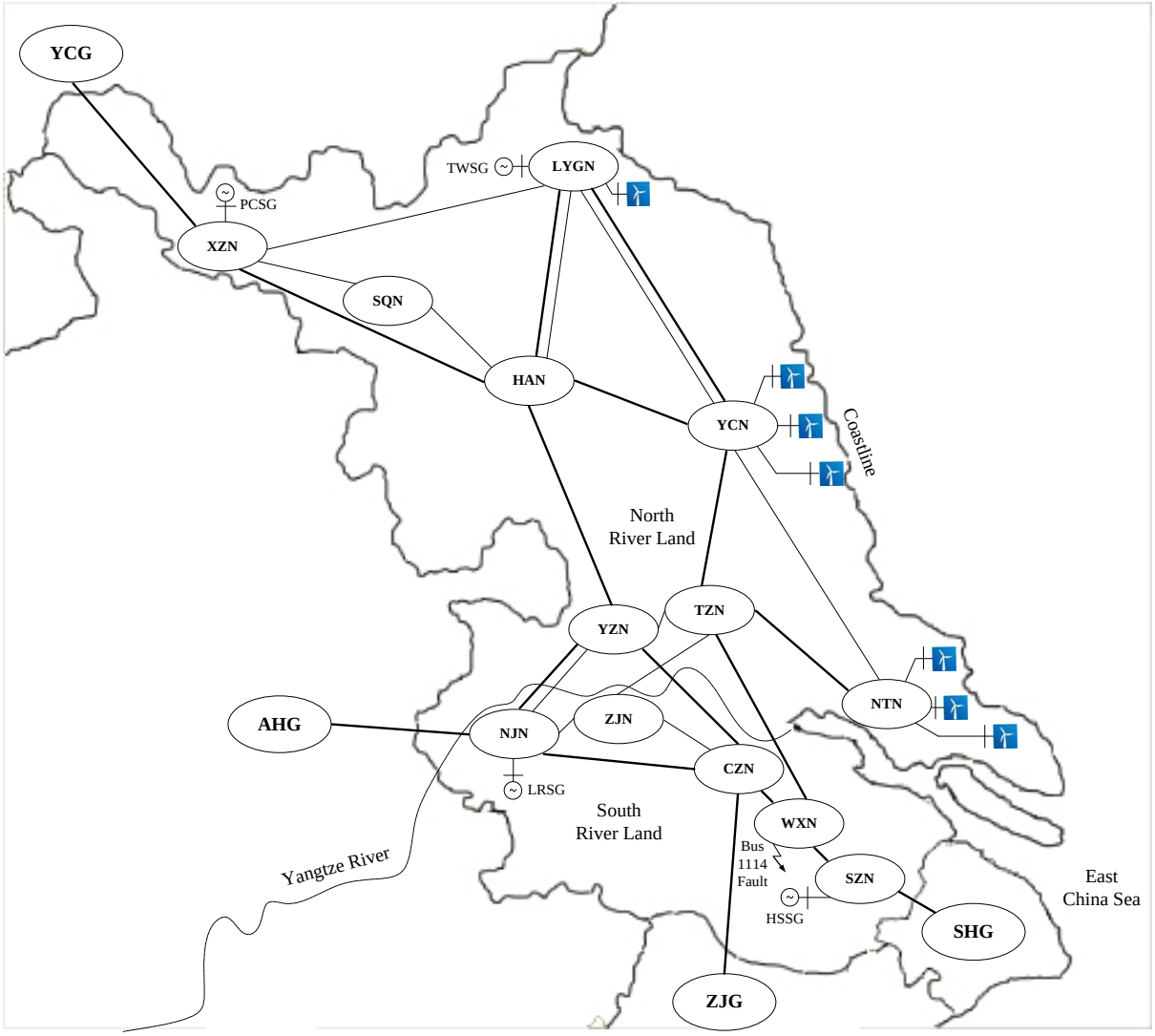

Fig. 9 Schematic diagram of 53-machine 1713-bus JS power grid integrated with 13 wind farms

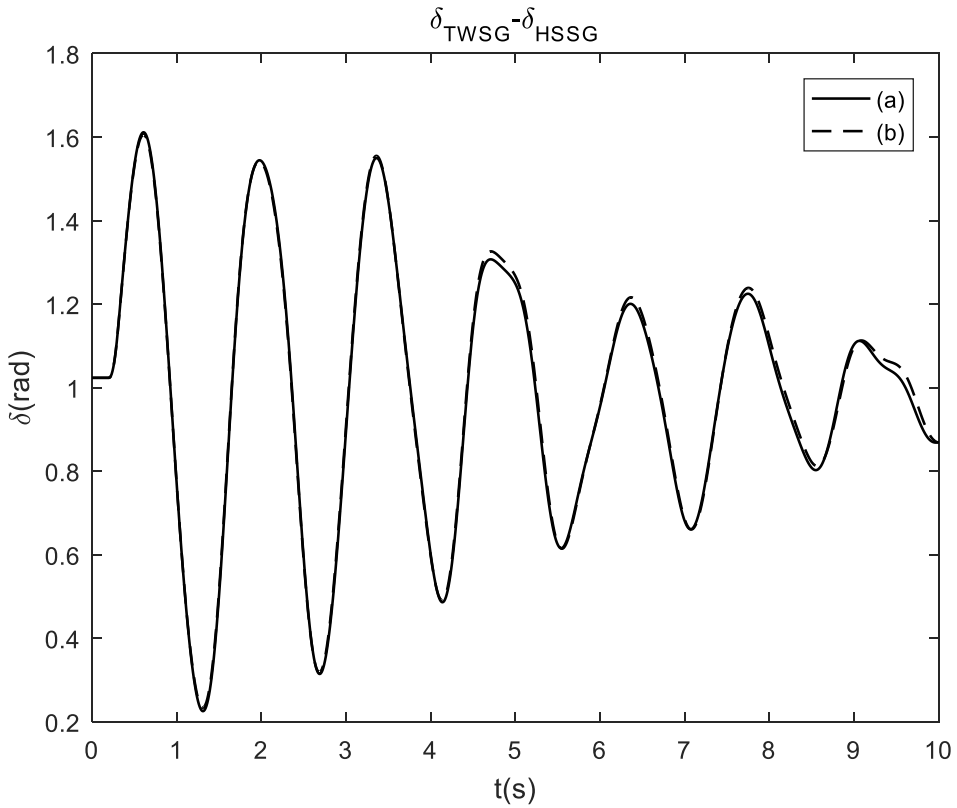

Fig. 10.1 TWSG-HSSG power angle difference with different wind farm dynamic models (a) 13 wind farms with detailed model (benchmark); (b) 13 wind farms with model reduction plans presented in Table 4

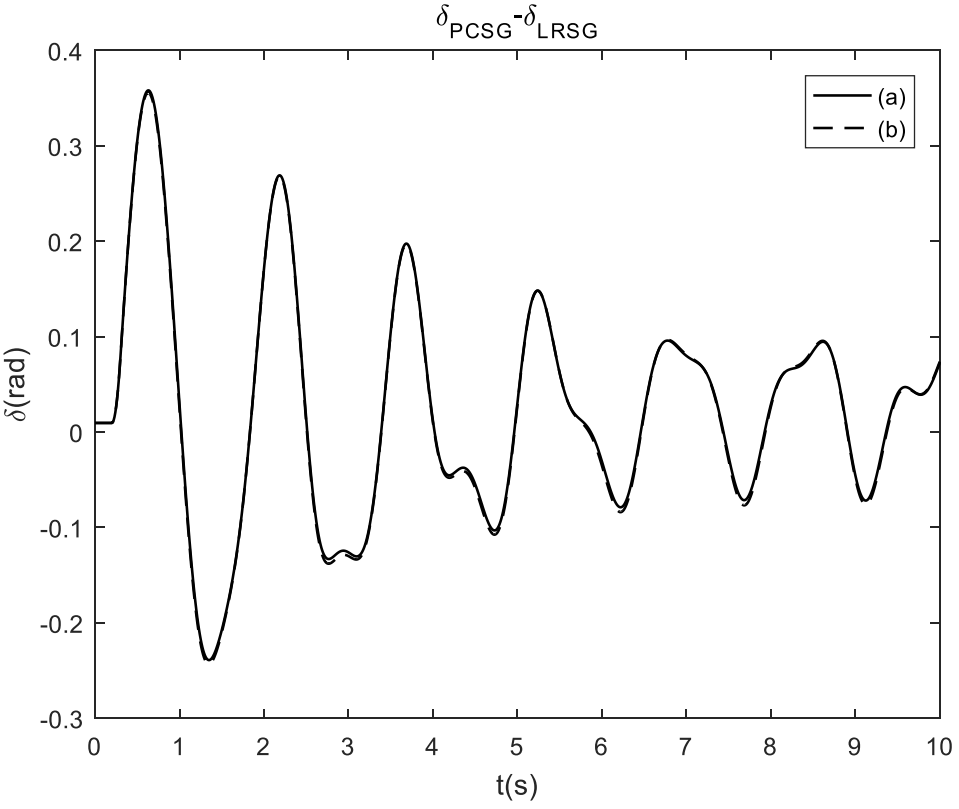

Fig. 10.2 PCSG-LRSG power angle difference with different wind farm dynamic models (a) 13 wind farms with detailed model (benchmark); (b) 13 wind farms with model reduction plans presented in Table 4

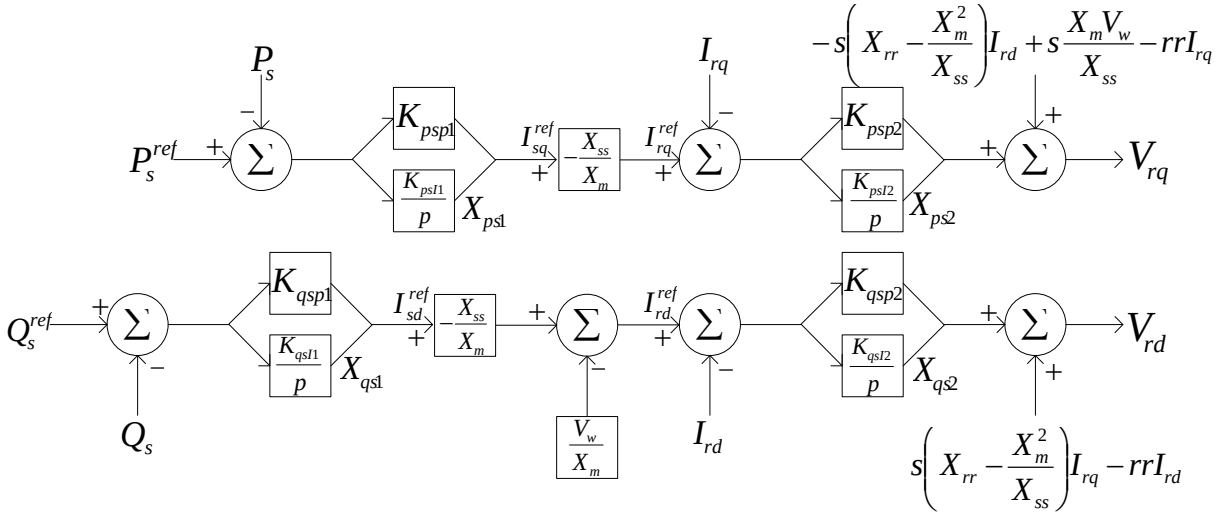

(a)

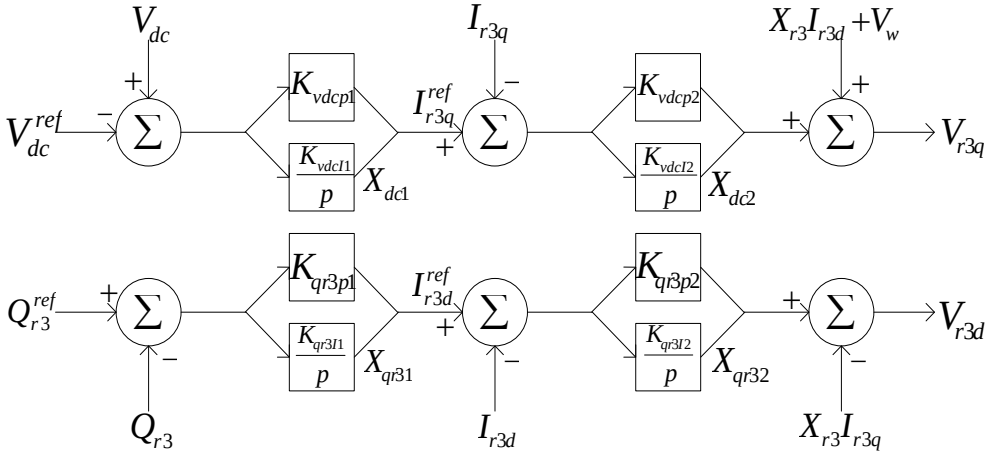

(b)

Fig. 11 DFIG converter control system models
(a) RSC controller model; (b) GSC controller model